Noise-assisted energy transfer in quantum networks and light-harvesting complexes

2010 New J. Phys. 12 065002

(http://iopscience.iop.org/1367-2630/12/6/065002)

New Journal of Physics
The open-access journal for physics

Noise-assisted energy transfer in quantum networks and light-harvesting complexes

A W Chin[1,4,5], **A Datta**[2,3], **F Caruso**[1,2,3], **S F Huelga**[1,4] **and M B Plenio**[1,2,3]

[1] Institut für Theoretische Physik, Universität Ulm, D-89069, Ulm, Germany
[2] Institute for Mathematical Sciences, Imperial College London, 53 Exhibition Road, London SW7 2PG, UK
[3] QOLS, The Blackett Laboratory, Imperial College London, Prince Consort Road, London SW7 2BW, UK
[4] Quantum Physics Group, Department of Physics, Astronomy and Mathematics, University of Hertfordshire, Hatfield, Hertfordshire AL10 9AB, UK
E-mail: alex.chin@uni-ulm.de

New Journal of Physics **12** (2010) 065002 (16pp)
Received 29 January 2010
Published 8 June 2010
Online at http://www.njp.org/
doi:10.1088/1367-2630/12/6/065002

Abstract. We provide physically intuitive mechanisms for the effect of noise on excitation energy transfer (EET) in networks. Using these mechanisms of dephasing-assisted transport (DAT) in a hybrid basis of both excitons and sites, we develop a detailed picture of how noise enables energy transfer with efficiencies well above 90% across the Fenna–Matthew–Olson (FMO) complex, a type of light-harvesting molecule. We demonstrate explicitly how noise alters the pathways of energy transfer across the complex, suppressing ineffective pathways and facilitating direct ones to the reaction centre. We explain that the fundamental mechanisms underpinning DAT are expected to be robust with respect to the considered noise model but show that the specific details of the exciton–phonon coupling, which remain largely unknown in these type of complexes, and in particular the impact of non-Markovian effects, result in variations of dynamical features that should be amenable to experimental verification with current or planned technology. A detailed understanding of DAT in natural compounds could open up a new paradigm of 'noise-engineering' by which EET can be optimized in artificial light-harvesting structures.

[5] Author to whom any correspondence should be addressed.

Contents

1. Introduction

The early stages of natural photosynthesis are able to capture and transport incident light energy with nearly 100% efficiency, and a clear understanding of these processes could be immensely valuable for optimizing the efficiency of artificial light-harvesting devices [1]. Ultrafast nonlinear spectroscopy has been used to probe energy transfer dynamics in the Fenna–Matthew–Olson (FMO) complex [2–4], a crucial part of the photosynthetic system of green sulfur bacteria. Recently, further experiments at physiological temperatures have been performed [5]. The FMO complex is an example of a pigment–protein complex (PPC), a network through which electronic excitations on individual pigments can migrate via excitonic couplings. It functions as a type of molecular 'wire' that funnels light energy captured in the chlorosome antennae to a reaction centre (RC), where the energy is used to initiate chemical reactions [6]. These experiments have demonstrated the existence of strong quantum coherences between multiple pigments, and have shown that the highly efficient energy relaxation in this system proceeds via coherently delocalized exciton states [2]. In addition, wave-like beating between these excitons has been observed to persist on timescales > 550 fs, a significant fraction of the typical transport time in FMO [3].

These observations have generated considerable interest in understanding the possibly functional role of quantum coherence effects in the remarkably efficient excitation energy transfer (EET) in FMO and other PPCs. It was initially argued that the fast transfer rates may be attributed to the exploitation of quantum search algorithms by the quantum dynamics of the FMO complex [1, 3]. However, typical timescales for relaxation and dephasing in PPCs [7] suggest that any quantum entanglement will be short ranged, and, as it is generally accepted that efficient quantum computation requires long-range entanglement [8], the application of the principles of standard quantum computation in this system is far from straightforward. As a result, the complete formulation of a possible link between quantum coherence and functionality is still an open problem [9–12].

Starting with the seminal work of [13–18], EET has been studied within the chemical physics community for several decades, yet the topic remains timely [19–22] due to the recent development of new experimental methods and also novel numerical techniques that allow theoretical models of the, still unknown, system–environment couplings to be tested [23]. Methods and ideas from quantum information science have also recently started to provide a new and complementary perspective on EET dynamics. Theoretical investigations of the role of

pure dephasing noise in EET have found that this noise has the ability to enhance both the rate and the yield of EET when compared to perfectly quantum coherent evolution [24, 25]. These results challenge the traditional view in information processing that noise always degrades the efficiency of quantum processes, and they demonstrate that controllable noise can even be considered as an additional engineering tool for tasks such as excitation transport [26].

In the exciton basis normally used in previous studies [27], dephasing-assisted transport (DAT) is understood as resulting from noise-induced transitions between exciton eigenstates that cause energetic relaxation of the excitations towards the RC. Though sufficient to suggest the possible existence of DAT in systems in contact with an uncontrollable environment, this approach does not currently describe in a transparent way *how* DAT actually works in detail and how it might be controlled or used. Such an understanding is essential for the fabrication of future artificial systems in which unavoidable noise might to some extent be employed as a constructive element to optimize light harvesting and transport [28, 29].

This paper revises and extends the physically intuitive picture we presented in [9] of how DAT, and more general noise-assisted transport, operates. It also highlights the engineering potential of deliberately applying noise in quantum transport networks. Starting with an idealized and exactly soluble model of noisy network transport, we revisit the underlying mechanisms that lead to DAT and then proceed to introduce additional complexity into this model to reveal how these mechanisms work in conjunction. Using these insights, we analyze simulations of EET in FMO using a hybrid basis that allows a novel and clear visualization of how these mechanisms operate in this system, and we also make quantitative predictions about how they can optimize the transport. In essence, it allows us to follow the evolution of the initial excitation across the molecular 'wire' as it makes its way to the RC. The exact nature of the hybrid basis is governed by the relative magnitudes of the site energies and their couplings to the neighbouring sites. In fact, it has recently (and independently) been used to explain the experimentally observed quantum coherences in the photosynthetic apparatus of cryptophyte algae at room temperature [30]. Finally, we expand upon previous descriptions of DAT in FMO to consider forms of non-Markovian dephasing and show that, although the fundamental mechanisms supporting DAT are robust with respect to the considered noise model, observable dynamical differences do appear that should be amenable to experimental testing. These types of evidence would be most valuable in discerning the exact nature of the exciton–phonon coupling in different types of photosynthetic complexes.

2. The network model

Following previous theoretical descriptions of PPCs [22, 24, 25], we consider the PPCs as networks composed of distinct sites, one of which receives a single initial excitation, while another is connected to the RC. The network of N sites is described by the coherent hopping Hamiltonian

$$H = \sum_{j=1}^{N} \hbar\omega_j \sigma_j^+ \sigma_j^- + \sum_{j\neq l} \hbar v_{j,l} (\sigma_j^- \sigma_l^+ + \sigma_j^+ \sigma_l^-), \tag{1}$$

where $\sigma_j^+ = |j\rangle\langle 0|$ and $\sigma_j^- = |0\rangle\langle j|$ are raising and lowering operators for site j, the state $|j\rangle$ denotes one excitation in site j and $|0\rangle$ is the zero exciton state. The local site energies are $\hbar\omega_j$, and $v_{j,l}$ are the coherent tunnelling amplitudes between the sites j and l. We do not assume

any particular form for the microscopic coupling that generates these tunnelling amplitudes and we therefore treat them as free parameters when considering abstract networks, as we do in section 3. For the case of the FMO complex, we will use the published Hamiltonian for *Prosthecochloris aestuarii* taken from [21], where the hopping parameters are fixed by the geometry and dipolar structure of the site interactions. We will further assume that the system is susceptible simultaneously to two distinct types of noise: a radiative decay process that transfers the excitation energy in site j to the environment (with rate Γ_j), and a pure dephasing process (with rate γ_j) that destroys the phase coherence of any superposition of localized excitations. The dynamics of the network's density matrix is modelled by a Markovian master equation of the form

$$\dot{\rho}(t) = -\mathrm{i}[H, \rho(t)] + \mathcal{L}_{\mathrm{rad}}(\rho(t)) + \mathcal{L}_{\mathrm{deph}}(\rho(t)), \tag{2}$$

where the local radiative and pure dephasing terms are described, respectively, by Lindblad super-operators $\mathcal{L}_{\mathrm{deph}}$ and $\mathcal{L}_{\mathrm{rad}}$,

$$\mathcal{L}_{\mathrm{deph}}(\rho) = \sum_{j=1}^{N} \gamma_j [-\{\sigma_j^+\sigma_j^-, \rho\} + 2\sigma_j^+\sigma_j^- \rho \sigma_j^+\sigma_j^-], \tag{3}$$

$$\mathcal{L}_{\mathrm{rad}}(\rho) = \sum_{j=1}^{N} \Gamma_j [-\{\sigma_j^+\sigma_j^-, \rho\} + 2\sigma_j^- \rho \sigma_j^+], \tag{4}$$

where $\{A, B\}$ denotes an anticommutator. Formally, this approach is equivalent to the Haken–Strobl model at infinite temperature [17], where pure dephasing is accounted for in terms of a classical, fluctuating field. The total excitation transfer is measured by the population transferred to the RC, modelled as the 'sink' node, numbered $N+1$, which is populated by an irreversible decay process (with rate Γ_{N+1}) from a site k of the network and described by a Lindblad operator $\mathcal{L}_{\mathrm{sink}}(\rho)$

$$\mathcal{L}_{\mathrm{sink}}(\rho) = \Gamma_{N+1}\left[2\sigma_{N+1}^+\sigma_k^- \rho \sigma_k^+\sigma_{N+1}^- - \{\sigma_k^+\sigma_{N+1}^-\sigma_{N+1}^+\sigma_k^-, \rho\}\right]. \tag{5}$$

The model is completed by introducing the sink population

$$p_{\mathrm{sink}}(t) = 2\Gamma_{N+1}\int_0^t \rho_{kk}(t')\,\mathrm{d}t', \tag{6}$$

which will be used as the key measure of the transport efficiency.

3. The fully connected network (FCN)

We shall show in the next few sections how the combination of inter-site coherence, interference of tunnelling amplitudes, and energetic disorder can conspire to drive strong DAT. For clarity, we begin by presenting each mechanism separately in simple network models in which these effects can be isolated. The first system we will consider is the FCN. The FCN is characterized by equal hopping strengths between all sites, i.e. $\hbar v_{j,l} = J$ for any $j \neq l$, and for the case of a uniform FCN, i.e. one in which ω_j, γ_j and Γ_j are the same on every site, an exact analytical solution for the density matrix for arbitrarily large networks can be found [9]. We first consider such a uniform FCN with $\gamma_j = 0$, $\Gamma_j = 0$, and one excitation on site 1. The

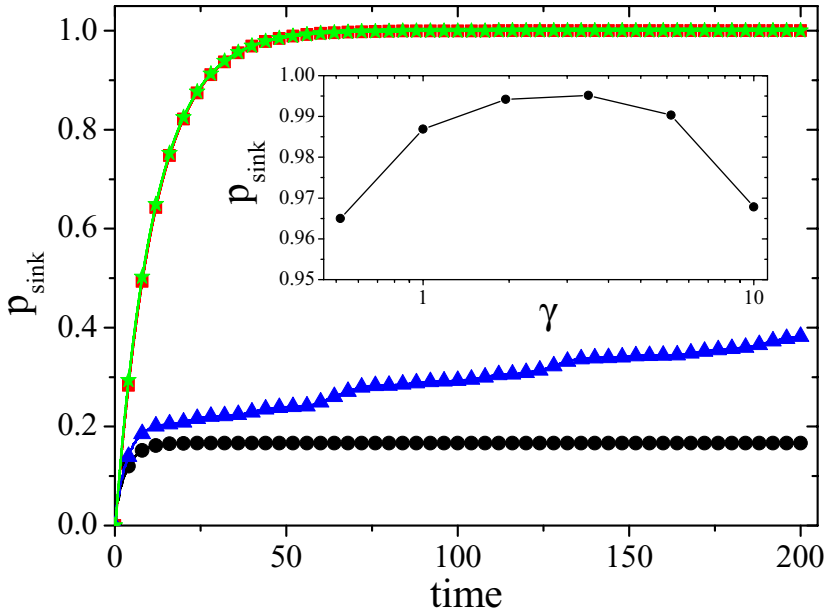

Figure 1. p_{sink} versus time for an FCN of $N = 7$ nodes with $\Gamma = 0$, $J = 1$, $\Gamma_{N+1} = 1$, for the cases of no dephasing (circles), pure dephasing (squares), static disorder (triangles) and static disorder with uniform dephasing (star). Destructive interference in the FCN can also be effectively removed (in the absence of pure dephasing) by the presence of static disorder in the local site energies or hopping rates. Such a disorder can prevent the cancellation of tunnelling amplitudes and thus enhances the asymptotic value of p_{sink}. For this case, the site energies are random numbers drawn uniformly from [0, 1], while the dephasing rates are chosen to equal 1 for all the sites in the dephasing case. Inset: $p_{\mathrm{sink}}(t)$ at a fixed time $t = 50$ as a function of γ.

only irreversible process left is the decay of population to the sink from site N. In figure 1, the time evolution of the sink population for these conditions is shown (circles) for the case of $N = 7$. This choice is motivated by the fact that the actual FMO complex that we will analyse in subsequent sections can be modelled as a seven-site network. In the absence of any noisy process, the asymptotic value of p_{sink} is $1/6$ and this should be contrasted with classical hopping for which $p_{\mathrm{sink}}(t \to \infty) = 1$. The striking difference between these results can be seen as a consequence of destructive interference of tunnelling amplitudes in the quantum case. Although individual sites have finite amplitudes J for transfer to other sites, a superposition state of the form $|\Psi_{ij}\rangle = (|i\rangle - |j\rangle)/\sqrt{2}$ cannot propagate in the network due to the perfect cancellation of the tunnelling amplitudes from each state in the antisymmetric superposition. This coherent trapping is illustrated in figure 2(a). Having identified these non-propagating states, the excitation asymptotically transferred to the sink can be understood as being just the weight of the initial state that lies outside the 'invariant subspace', which consists of all $|\Psi_{ij}\rangle$ that have zero tunnelling matrix elements with the localized state $|N\rangle$ and therefore do not feel the presence of the sink. For the case considered here, this insight immediately predicts $p_{\mathrm{sink}}(\infty) = 1/(N-1)$, in agreement with the result shown in figure 1. Invariant subspace analysis of more complex networks and other initial conditions can be found in [9].

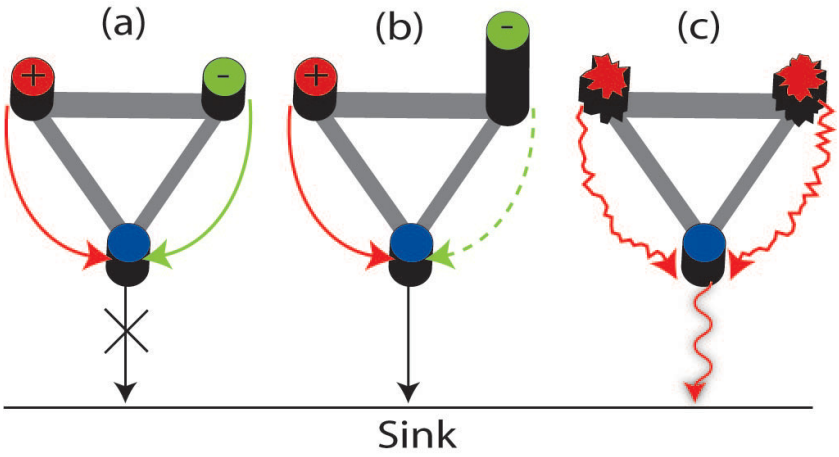

Figure 2. A three-site FCN. In (a), destructive interference of the tunnelling amplitudes from each site in an antisymmetric eigenstate prevents transfer to the sink site (blue). In (b), an energy mismatch generates an asymmetric stationary state, which is coupled to the sink and leads to transport. In (c), local dephasing efficiently removes destructive interference effects and generally leads to excitation transfer to the sink at a faster timescale than mere energy disorder.

Purely coherent dynamics can thus impede transport in multiply connected networks via interference, but, in the presence of dephasing noise, trapped excitations can become propagating, as shown in figure 2(c). This is the first physical mechanism of DAT: the *removal of transport-suppressing interference effects*. Figure 1 shows that, as the dephasing noise strength γ increases, the efficiency rapidly rises to near-perfect excitation transfer as the phase coherence of the $|\Psi_{ij}\rangle$ states is destroyed. With further increase in γ, the efficiency drops as noise suppresses tunnelling via the quantum Zeno effect, as shown in the inset of figure 1. We thus find an optimum dephasing strength where the combination of coherent tunnelling and dephasing maximizes the transport efficiency, a generic feature of networks that display DAT, as we will discuss again in the context of the FMO dynamics. This coherent trapping and DAT are related to the type of 'dark states' found in quantum dot and optical systems [31–33]. If we allow in our model for site energies to become disordered, another mechanism of DAT appears: *line broadening*. Random energetic disorder removes the destructive interference discussed above, and formally leads to $p_{\text{sink}}(\infty) = 1$ in the absence of noise. Note, however, the different timescale of the process, as illustrated by the triangles sequence in figure 1. If the energy difference between sites is much greater than their coherent couplings, the energy eigenstates are effectively localized, and coherent transport between these sites is strongly suppressed. Thus EET times may be very long and excitations may decay before reaching the target [9]. However, pure dephasing causes spectral broadening of the site energies, and, if it is sufficiently strong to cause overlap of site energies, additional incoherent tunnelling between sites can be activated, leading to an increase in EET efficiency, as shown in figure 1 (stars). Line broadening is also the basis for the Forster mechanism, which is frequently used to study EET in chromophoric systems and has been well understood for some time [13].

It is important to note that highly efficient DAT is not simply achieved by using noise to drive the dynamics into a purely classical regime; rather it is a combination of both noise and

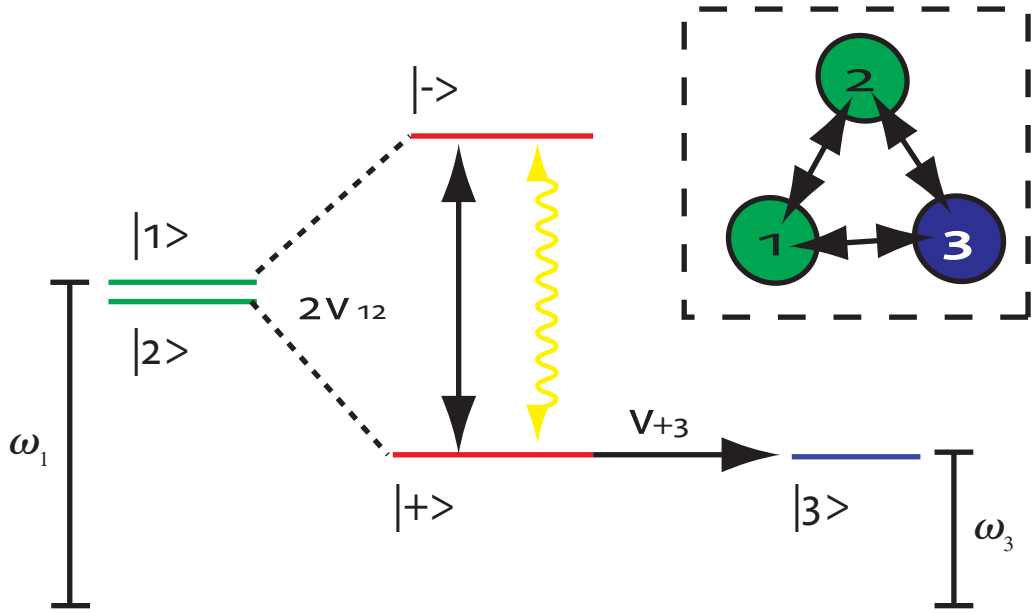

Figure 3. Energy level and coupling structure in a hybrid basis for a three-site FCN (inset). Coherent couplings are shown by straight arrows. Tuning v_{12} can bring the $|+\rangle$ state into resonance with site 3 leading to fast transport. The $|-\rangle$ is uncoupled from site 3, but noise induces incoherent transitions between $|-\rangle$ and $|+\rangle$ (corrugated arrows), allowing populations initially held in $|-\rangle$ to also utilize the fast $|+\rangle \rightarrow |3\rangle$ pathway.

coherence, which places the system at the boundary between quantum and classical physics, thus making DAT much more efficient than purely coherent dynamics. This interplay and its possible use for optimizing transport efficiencies can be simply illustrated using a hybridized basis set to look at a slightly non-uniform three-level FCN with couplings $v_{13} = v_{23}$ and site energies $\omega_1 = \omega_2 \neq \omega_3$. Expressing the FCN Hamiltonian in the basis $\{|+\rangle, |-\rangle, |3\rangle\}$, where $\sqrt{2}|\pm\rangle = |1\rangle \pm |2\rangle$, leads to the new level and coupling structure shown in figure 3. This figure shows how the system can exploit coherence to alter the energy landscape via the coherent splitting of the $|\pm\rangle$ states and also to change the hopping matrix elements between states. In this example, the inter-site coherence can be chosen to create a highly efficient transport pathway to the sink by bringing the $|+\rangle$ state into resonance with $|3\rangle$ and enhancing the tunnelling amplitude. However, the other state becomes decoupled from site 3 due to larger energy mismatch and, in this particular case, cancellation of tunnelling matrix elements. Population in this state is decoupled from the sink. Now, adding noise to the system dephases superpositions of localized states $|i\rangle$, and in the hybrid basis this opens an incoherent transition between $|-\rangle$ and $|+\rangle$. When noise is weak enough to preserve the coherent level structure for sufficiently long times, the population initially in $|-\rangle$ can therefore also take advantage of the fast resonant $|+\rangle \rightarrow |3\rangle$ transfer, leading to a large DAT effect.

4. Light-harvesting molecules (the FMO complex)

Having presented some underlying mechanisms of noise-assisted EET in the FCN models, we now investigate in detail how they operate in the FMO complex [6]. The FMO complex is a trimer of three identical units, each composed of seven bacteriochlorophyll *a* molecules

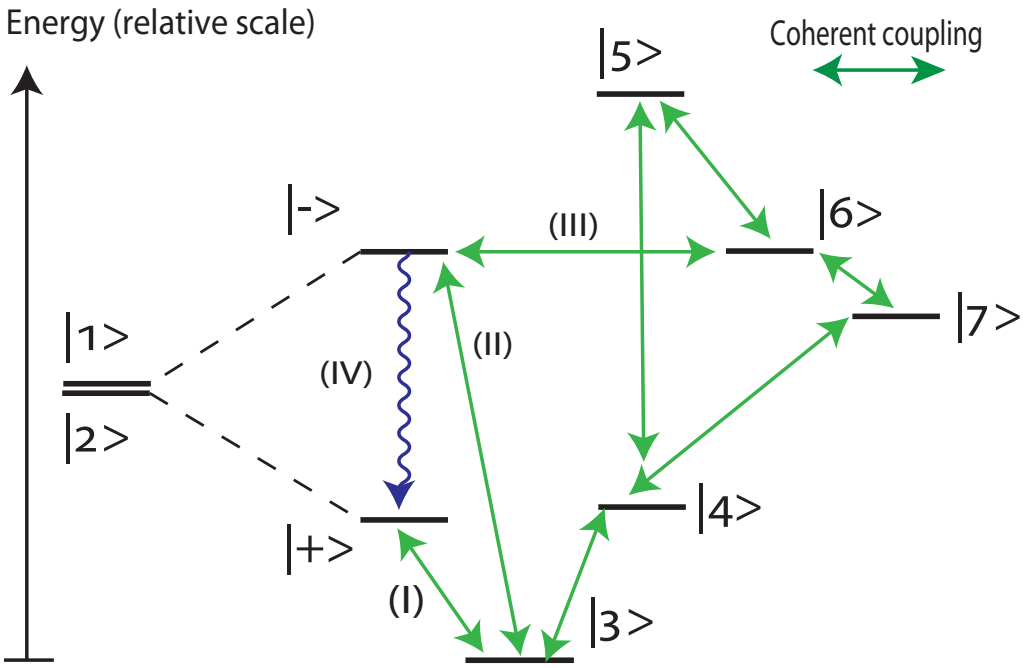

Figure 4. Energy level structure of the FMO Hamiltonian in the hybrid basis described in the text. Only the most significant coherent couplings are shown (green lines), and the coherent interactions that dominate the dynamics in the absence of noise are labelled (I)–(III). For FMO, site 3 is coupled directly to the sink. The most important new transport pathway arising from the presence of noise is labelled (IV). (a) Population in $|+\rangle$ decays quickly into the sink due to nearly resonant coherent interaction with site 3. (b) Coherent coupling of $|-\rangle$ gives slow population transfer due to a large energy mismatch with site 3. (c) Resonant coherent coupling causes strong population oscillations between $|-\rangle$ and sites 5–7, inhibiting transfer to the sink in the absence of noise. This pathway is suppressed by dephasing and enhances transport. (d) In the hybrid basis, a pure dephasing noise opens an incoherent relaxation channel, which allows the population of the $|-\rangle$ state to decay into the $|+\rangle$ state and then quickly decay into the sink via path (a).

embedded in a scaffolding of protein molecules. We model the FMO monomer unit as a seven-site network with coupling strengths and site energies taken from [21]. The typical EET timescale is known to be of several picoseconds, which is much shorter than the 1 ns typical radiative lifetime of excitons. The excitation starts on site 1, thought to be the site closest to the base plate, and site 3 is connected to the RC (sink). Our numbering of the FMO sites follows the conventional one [6, 21]. The excitation transfer in the FMO complex of *P. aestuarii* undergoing completely coherent dynamics is shown by the green line in figure 7 and only reaches 57% over the typical transfer time of 5 ps. This dephasing-free evolution resembles the FCN case shown by the sequence of circles in figure 1 and can be explained using a similar picture.

The strong coupling between sites 1 and 2 in the FMO Hamiltonian inspires a hybrid basis $\{|+\rangle, |-\rangle, |3\rangle \ldots |7\rangle\}$, where $|\pm\rangle = 1/\sqrt{2}(|1\rangle \pm |2\rangle)$. In this basis, the Hamiltonian has the local site energies and coupling structure shown in figure 4. An initial excitation on site 1

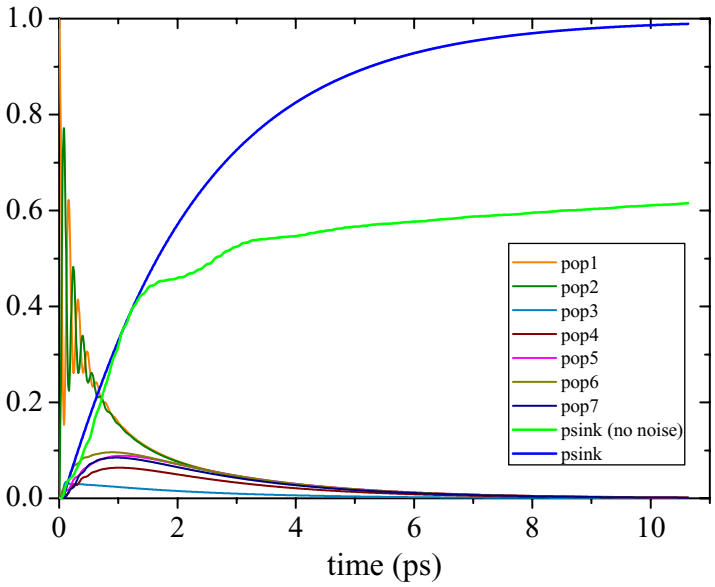

Figure 5. Site populations versus time (in ps) for the FMO complex subject to optimized Markovian dephasing noise. We also show p_{sink} for the noiseless case (light green line) and the transfer efficiency for the Linbladian noise model with optimized dephasing rates (blue line). For the optimized decay rates, the transport is nearly complete within the experimental 5 ps transport time, and coherent oscillations in the dynamics persist until 1 ps.

corresponds to the initial condition $\sqrt{2}|1\rangle = |+\rangle + |-\rangle$. As in the FCN example, the strong coherent interaction between sites 1 and 2 pushes the $|+\rangle$ state closer in energy to state $|3\rangle$ and, as shown in figure 4, the population in this state decays quickly into the sink via path (I). Note, however, that there is a relatively small coherent enhancement or cancellation of the transition amplitudes between $|\pm\rangle$ and $|3\rangle$ as $v_{13} \ll v_{23}$. The near resonance of the $|+\rangle$ state represents the dominant contribution to the initial fast rise in p_{sink} in the noise-free case, as shown in figure 5.

Once $\sim$50% of the excitation initially in $|+\rangle$ has decayed, the rise time of p_{sink} becomes much slower as the population initially in $|-\rangle$ does not propagate as efficiently into site 3. To understand this we need to examine the two principal remaining paths, (II) and (III) in figure 4. The $|-\rangle$ state has roughly the same coupling strength to site 3 as the $|+\rangle$ state; however, it is at a much higher energy. By turning-off all couplings in the Hamiltonian so that only path (II) is active, we are able to measure the isolated population transfer rate via this path, and find that it is over an order of magnitude slower than the decay rate via path (I) in the absence of noise. The second process (path (III) in figure 4) would be obscured in a full site or exciton basis, but reveals itself very clearly in the hybrid picture. As seen in figure 4, $|-\rangle$ is almost resonant with site 6, and, as a result of *constructive* interference of the tunnelling amplitudes v_{16} and v_{26}, the effective coupling of $|-\rangle$ and $|6\rangle$ is about twice the energy mismatch of these states.

This strongly coupled resonance causes the population held in state $|-\rangle$ to oscillate across the complex between sites 1 and 2 and site 6. Sites 5 and 7, which are strongly coupled to 6, also participate in these oscillations, and these oscillations are shown in figure 6(a). Direct and indirect coherent transport from sites 5–7 to the sink are even slower than path (II), and these oscillations along path (III) dominate the dynamics and effectively prevent this population from

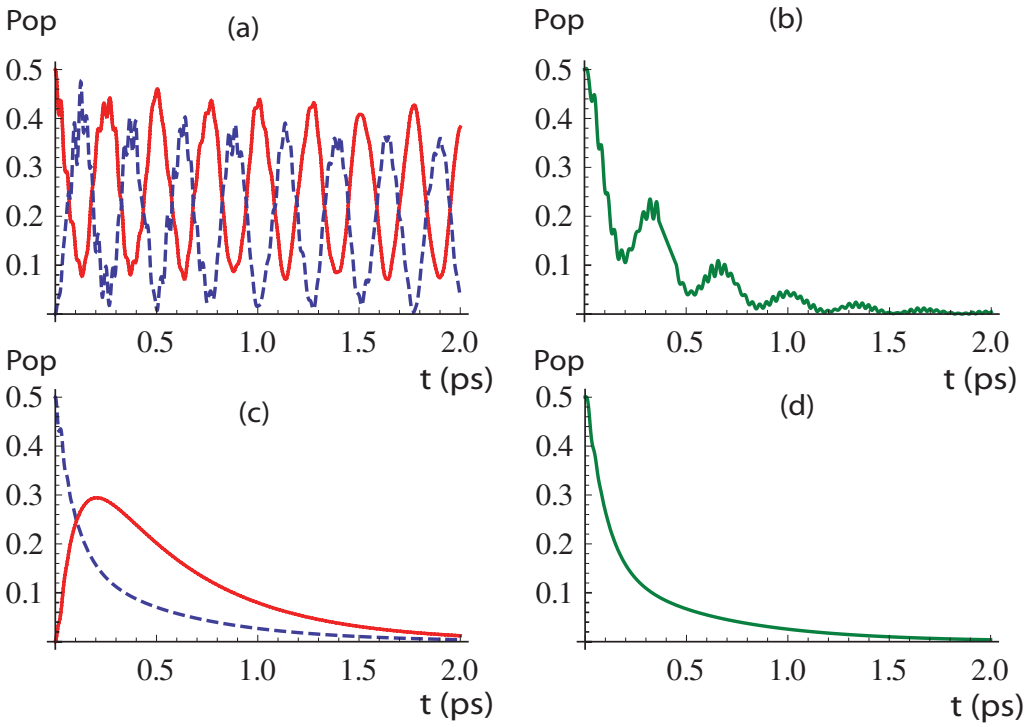

Figure 6. (a) Population of the $|-\rangle$ state (red line) and the combined populations of sites 5–7 (blue dashed line) as a function of time for the case of no dephasing noise. These populations coherently oscillate due to the resonant coupling of $|-\rangle$ to site 6. (b) The population of the $|+\rangle$ state in the absence of dephasing. The $|+\rangle$ is close to a direct resonance with site 3 and this population decays rapidly. This gives the fast initial rise time of p_{sink} in the absence of dephasing. (c) Population of the $|-\rangle$ state (red line) and the combined populations of sites 5–7 (blue dashed line) as a function of time with optimized dephasing rates. Coherent oscillations between $|-\rangle$ and $|5\text{–}7\rangle$ are suppressed and the population in the $|-\rangle$ states decays rapidly through the incoherent $|+\rangle \rightarrow |3\rangle$ path described in the text. (d) The population of the $|+\rangle$ state with optimized dephasing rates. Oscillatory features are washed out compared to the case of no dephasing, although the average decay rate is similar to case (b). Note also that, with the optimized dephasing rates, the decay of the $|-\rangle$ state has almost the same time dependence as the $|+\rangle$ state.

decaying into the sink via path (II). To obtain an estimate of the importance of these oscillations, we compare the average rate of change of $p_{\text{sink}}(t)$ (after the initial fast decay) for the full FMO Hamiltonian, and the same Hamiltonian with the coupling between $|-\rangle$ and site 6 set to zero. We find that in the latter case the transfer rate becomes 50% larger than the former case.

The blue line in figure 5 shows the transport obtained with dephasing rates that were optimized numerically for a transfer time of about 5 ps [9] and which cause p_{sink} to increase to 0.903 over this timescale. This dramatic increase in EET arises primarily from the noise-induced suppression of pathway (III) in figure 4 and the new noise-induced incoherent transition between $|-\rangle$ and $|+\rangle$, shown as path (IV) in figure 4. Path (IV) allows the population initially in the $|-\rangle$ state to decay via the fast $|+\rangle \rightarrow |3\rangle$ path (I). In fact, we find that dephasing on sites 1

and 2 alone is sufficient to drive p_{sink} to about 0.85. The remaining improvement in efficiency in our optimized simulations arises from strong dephasing on sites 3–7. Dephasing on sites 5–7 (along with dephasing on sites 1 and 2) destroys the coherent oscillations that keep the initial $|-\rangle$ population away from the trap in the noiseless case, and the resulting incoherent transitions along path (III) rapidly redistribute this population equally among states $|-\rangle$ and $|5\rangle$–$|7\rangle$. Line broadening due to dephasing on sites 3–7 quickly transfers populations from sites 5–7 to the sink via sites 4 and 3, and noise on site 3 further enhances the EET rate via line broadening effects on paths (I) and (II) of figure 4. The suppression of the $|-\rangle \rightarrow |6\rangle$ oscillations and the stronger decay of the $|-\rangle$ population via path (I) of figure 4 are shown in figures 6(c) and (d). Most importantly, it is not necessary for the dephasing parameters to be exactly equal to the values obtained by optimization. Large variations in these values still lead to essentially the same evolution of the population in the sink. However, the values used to obtain figure 5 do give coherent oscillations that last up to about 1 ps, which is roughly consistent with the experimentally observed coherence time (>600 ps) seen in FMO at 77 K. Similar robustness is also seen for variations in site energies and inter-site couplings. This sort of robustness and effectiveness over a broad range of parameters is essential for the notion of noise-assisted transport to operate in natural conditions.

Although there is no direct evidence that natural evolution has performed such a full optimization of the EET process with respect to dephasing noise [34], the analysis above provides a good example of how one could, in principle, optimize EET in an artificial system. By identifying the naturally effective and inefficient pathways, one could apply noise selectively to create new pathways to circumvent the inefficient ones using the efficient paths, as in path (IV), enhance the efficient paths with line broadening, as in path (I) or even remove unwanted coherent dynamics, such as path (III).

While the microscopic interaction parameters of the FMO pigments and the protein environment are not well characterized experimentally, our local Markovian description of the noise neglects a number of potentially important processes, and we now consider two of these. One of these is the role of spatial correlations in the process of EET. The other is the presence of temporal correlations or memory in the environment that can lead to altered exciton dynamics, which are not necessarily governed by a Lindblad-type master equation. The first of these, spatially correlated noise, can be modelled via the Lindblad term

$$\mathcal{L}_{\text{deph}}(\rho) = -\sum_{mn} \gamma_{mn}[A_m, [A_n, \rho]], \tag{7}$$

where $A_m = \sigma_m^+ \sigma_m^-$. After a full optimization of all γ_{mn}, we find that p_{sink} saturates at 0.931 after 5 ps. This small improvement indicates that non-local effects may be of limited importance for EET in the FMO complex. However, there is experimental evidence for strong spatial correlations in bacterial RC dynamics [35] and conjugated polymers [36], and correlated noise has also been predicted to be relevant in other photosynthetic complexes [37].

5. Non-Markovian models

In this last section, we focus on analyzing the possible impact on EET dynamics of deviations from the Markovian model that we presented in the previous sections. As stressed before, the theoretical model used in the previous sections treats pure dephasing in a way equivalent to the phenomenological Haken–Strobl model. However, a number of recent studies of EET in FMO

have looked at the effects of different microscopic models of the exciton–phonon interaction on the dynamics, and in particular at the non-Markovian dynamics arising from strong coupling and/or the form of the spectral function of the environment [10, 11, 38–40]. In this section, we shall consider the structured bath spectral density used by Adolphs and Renger in [21]. This spectral density contains a contribution from a low-energy continuous density of states and a discrete high-energy mode, and its effects on the dynamics of a dimer molecule have recently been simulated using a new and numerically exact application of the time-adaptive density matrix renormalization group (t-DMRG) method [38]. This study showed that the coupling to the high-energy mode can lead to oscillations in the dimer population dynamics that persist over the whole transport time and, moreover, that the efficiency of inter-site transfer in the presence of these oscillations is just as high as when the high-energy mode is decoupled from the dimer. In order to see if this coexistence of long-lasting oscillations and efficient transport can operate in more complex networks, we now go beyond the dimer setting of [38] and look at the effects of local mode couplings on the EET dynamics of FMO.

We will focus here just on the discrete part of the spectral density and consider a model in which each FMO chromophore is linearly coupled to a harmonic mode with frequency $\omega_{\mathrm{H}} = 180\,\mathrm{cm}^{-1}$, with strength $g = \sqrt{S_{\mathrm{H}}}\omega_h$ and $S_{\mathrm{H}} = 0.22$, following [21]. To describe these couplings, we add to the previous Hamiltonian in equation (1) the following two terms:

$$H_{\mathrm{B}} = \sum_{j=1}^{7} \hbar\omega_h a_j^{+} a_j, \qquad H_{\mathrm{SB}} = \sum_{j=1}^{7} g(a_i + a_i^{+})\sigma_j^{+}\sigma_j^{-}, \tag{8}$$

with H_{B} being the free Hamiltonian for the two-level bath with creation and annihilation operators a^{+} and a, respectively, and mode frequency ω_{H}, whereas H_{SB} is the system–bath interaction Hamiltonian with interaction strength g. We note that the frequencies and interactions strength of the couplings predict a reorganization energy, a measure of the coupling strength to the localized mode, of $S_{\mathrm{H}}\omega_{\mathrm{H}}$, which corresponds to a mode occupation of just $S_{\mathrm{H}} = 0.22$ when the mode relaxes into equilibrium with respect to the exciton-mode interaction at $T = 0\,\mathrm{K}$ on a single isolated chromophore with a single excitation present. It is therefore reasonable to consider the local modes within a two-level approximation, and numerically monitoring the populations in each local mode confirmed that no local modes were strongly excited or saturated over the whole time interval of the simulations. We also consider the case in which each bath mode can be damped with a damping rate Γ, which gives a smooth spectral width to the bath density of states and hence a decay of the correlation time of the environment. When this damping is large, the bath spectral density is essentially unstructured in frequency space and induces a purely Markovian dissipation on the exciton dynamics. The damping is introduced by considering a Lindblad term $\mathcal{L}_{\mathrm{rad}}^{\mathrm{bath}}(\rho)$ of the form as in equation (4), with the same rate Γ for all the local baths.

In figure 7, we show the site population behaviour as a function of time for the case of $\Gamma = 1$ and the transfer efficiency p_{sink} for different values of Γ. Coupling to lightly damped coherent modes ($\Gamma = 1$) gives a very large improvement of the transport, as compared with the noiseless case, with $p_{\mathrm{sink}} \sim 0.95$ at 5.5 ps. This is close to complete transfer. Note that for this case the populations, notably in sites 1 and 2, display strong oscillations for up to 5.5 ps, i.e. the whole transport time. This is perhaps interesting as it shows that persistent oscillations are not necessarily inconsistent with fast and total transport. This should be contrasted to the Lindblad dephasing model of the previous sections, in which we found that excitonic coherences are observable only over the first 20% of the total transport time when the transport is

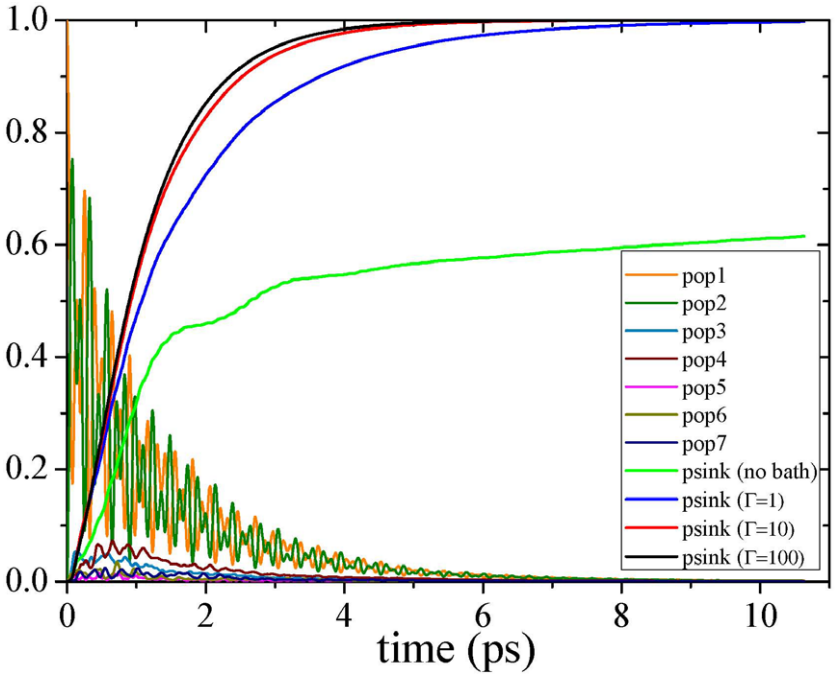

Figure 7. Site population and p_{sink} versus time (in ps) for the FMO complex. We show the noiseless case (light green line) and the transfer efficiency for a non-Markovian model where each site is coupled to a structured phonon bath, as specified in [21], and for different values of the local bath damping rate Γ expressed in spectroscopic units (cm^{-1}). The site population behaviour is plotted for $\Gamma = 1$ while oscillations are strongly suppressed for larger values of Γ.

optimized. Another interesting observation is that this non-Markovian model appears to be able to implement the enhancement and suppression of pathways through the FMO energy landscape very well, better in fact than the optimized Markov case. Comparing figures 5 and 7, we see that, in the local mode simulation, the bath strongly suppresses the transfer of populations from sites 1 and 2 to sites 5–7 that occurs via the resonant path (III) in figure 4 in the absence of noise. While Markovian noise eventually destroys these coherent oscillations 'across the molecule', there is still a substantial leakage via incoherent tunnelling into sites 5–7 and their total population reaches as high as 0.3 at 1 ps. In the local mode case, the total population of sites 5–7 never rises above 0.05. Apart from sites 1 and 2, the only sites to become significantly populated are sites 3 and 4, which are closely linked to the sink. The local modes seem to localize the excitations more effectively around the sink and prevent the exploration of inefficient paths, like (III) in figure 4.

From the point of view of noise engineering, it seems that the application of non-Markovian, quantum noise might allow for a more precise control of the direction and speed of the dynamics. However, it remains to be shown that the strong effect we see is not just due to a fine-tuning of exciton and mode parameters in the Hamiltonian, i.e. we would like to see how robust this non-Markovian DAT is. This point can be partially investigated by looking at the damping of these modes. As illustrated in figure 7, damping the modes leads to an incremental improvement in the transport efficiency as the damping rate Γ acting on each site is increased from the value $\Gamma = 1$ (blue curve) to $\Gamma = 10$ (red) and $\Gamma = 100$ (black). This

incremental improvement in transport efficiency coincides with increasingly fast decay of the oscillations of the population dynamics (not shown). This shows that the long-lasting population oscillations in this noise model, which are seen for weak mode damping, are likely to involve exciton coherences mediated by the local modes.

Increasing the damping of the local modes makes the effective environment seen by the excitons more Markovian in nature and leads to increases in the transport efficiency, as evidenced by the behaviour of p_{sink}. This conclusion that increasing Markovianity increases the transport rate differs from the one obtained within a different noise model put forward recently in [39], where an enhancement of the transfer rate was observed when the exciton–bath interaction was treated without the Markov approximation. It seems clear that linking Markovian or non-Markovian effects to an improved or slowed down transfer is not straightforward and strongly depends on specific features of the noise model being considered; and perhaps there is no universal, model-independent, relation between non-Markovian effects and efficiency of EET. As a result, we can conclude that, while the process of EET in FMO is clearly noise assisted, in the sense that evolution under the exciton Hamiltonian alone cannot account for the observed transport efficiency, the EET dynamics and the transport efficiency as measured by p_{sink} are very sensitive to the specific noise model. In particular, efficient transport with long-lasting oscillations might arise from any combination of weak Markovian damping, slow, non-Markovian environments, as in [10, 40], spatially correlated baths [36] or coupling to local modes, as shown here.

As the role of noise is clearly crucial for efficient EET, further experimental results are needed to discriminate between these different noise models. One important issue related to this is whether or not, at physiological temperatures, the net effect of the dephasing due to the coupling of the complex to the protein environment can be modelled in terms of a classical, fluctuating field or must be treated explicitly as a *quantum environment*. The dynamical behaviour of quantum correlations among the excitons [11], and also between the bath and exciton system [41], is also expected to be sensitive to the noise model, and the recent formulation of efficient techniques for the tomographic characterization of many-body systems [42] may allow for experiments that can directly probe the nature of the exciton–protein coupling in photosynthetic complexes.

6. Conclusions

We have revisited the basic mechanisms by which pure dephasing noise can open up or suppress pathways through the energy landscape of a quantum network, and we have shown how these processes can dramatically increase the efficiency of EET relative to their noiseless evolution. Using these insights, we constructed a hybrid basis for analysing the FMO dynamics and indicated the key pathways that are responsible for the inefficiency of the EET in the absence of noise. For excitations to propagate efficiently, these pathways must be either avoided or inhibited, and we have shown within a fully Markovian approach how pure dephasing noise achieves this and how it effects each of the principal pathways individually. As the identification of the transport-suppressing pathways is made without any reference to the noise model, we believe that any noise model that enhances transport must more or less carry out this strategy of suppressing the inefficient paths and enhancing the direct relaxation channels. This intuition is supported by our results using the non-Markovian local mode model, where we find a very effective suppression of the inefficient pathways, leading to a transport time that can even

exceed the optimized Markovian dynamics. The results obtained from these models emphasize how knowledge of the underlying Hamiltonian, when expressed in an appropriate basis, might allow the possibility of using applied noise almost as an engineering tool for the creation of artificial light-harvesting architectures. Although we have demonstrated the technique for the FMO complex, we could use such a path analysis to quite literally follow the movement of the excitation across any network to the sink, and enhance the energy flow with selective application of appropriate noise interactions.

We have also shown in our local mode noise model that the experimentally observed transfer time can occur through dynamics that preserve coherences and entanglement across the whole transport time. The optimized Markovian theory can only preserve coherences for 20% of this time. The potential relevance of this observation for understanding the long-lasting coherences observed in FMO and other photosynthetic complexes still remains unclear, and, in particular, the effects of temperature must be understood before a connection to the experimental data can be made. However, this model provides a new, interesting system for studying *quantum noise*-assisted transport and further emphasizes one of the underlying messages of this paper, which is: the necessary tasks for enhancing exciton transport revealed by our path analysis can be achieved by a wide variety of noise models, each of which can generate very different dynamics. As noise is a crucial part of the efficiency of EET in photosynthetic complexes, there is a need for experimental discrimination of noise models. Such studies would also provide clues to the still unanswered question of whether quantum mechanics, in the form of coherence and entanglement, is necessary for EET or whether it is just an inevitable consequence of quantum mechanical evolution on the short lengths and timescales found in PPCs. To answer this question requires further studies on energy transport across connected networks in the presence of various noise models, with interesting ramifications for the role of coherence and entanglement in the dynamics of interacting systems.

Acknowledgments

This work was supported by the EPSRC QIP-IRC, EPSRC grant number EP/C546237/1, EU projects QAP and CORNER, the von Humboldt Foundation and the Royal Society. We are grateful to G R Fleming, A Ishizaki, S Virmani and T Brandes for helpful discussions and comments. F C was also supported by a Marie Curie Intra European Fellowship within the 7th European Community Framework Programme.

References

[1] Sension R J 2007 *Nature* **446** 740
[2] Brixner T *et al* 2005 *Nature* **434** 625
[3] Engel G R *et al* 2007 *Nature* **446** 782
[4] Lee H *et al* 2007 *Science* **316** 1462
[5] Panitchayangkoon G *et al* 2010 arXiv:1001.5108
[6] Olson J M 2004 *Photosynth. Res.* **80** 181
[7] Abramavicius D *et al* 2008 *Biophys. J.* **94** 3613
[8] Jozsa R and Linden N 2003 *Proc. R. Soc.* A **459** 2011
[9] Caruso F *et al* 2009 *J. Chem. Phys.* **131** 105106
[10] Ishizaki A and Fleming G R 2009 *Proc. Natl Acad. Sci. USA* **106** 7255

[11] Caruso F *et al* 2009 *Phys. Rev.* A at press arXiv:0912.0122
[12] Fassioli F and Olaya-Castro A 2010 arXiv:1003.3610
[13] Förster T 1948 *Ann. Phys. Lpz.* **2** 55
[14] Redfield A G 1965 *Adv. Magn. Reson.* **1** 1
[15] Grover M and Silbey R J 1971 *J. Chem. Phys.* **54** 4843
[16] Pearlstein R M 1972 *J. Chem. Phys.* **56** 2431
[17] Haken H and Strobl G 1973 *Z. Phys.* **262** 135
[18] Kenkre V M and Knox R S 1974 *Phys. Rev. Lett.* **33** 803
[19] Scholes G D 2003 *Annu. Rev. Phys. Chem.* **54** 57
[20] Ishizaki A and Fleming G R 2009 *J. Chem. Phys.* **130** 234111
[21] Adolphs J and Renger T 2006 *Biophys. J.* **91** 2778
[22] Cheng Y C and Fleming G R 2009 *Annu. Rev. Phys. Chem.* **60** 241
[23] Ishizaki A and Tanimura Y 2005 *J. Phys. Soc. Japan* **74** 3131
Bulla R *et al* 2003 *Phys. Rev. Lett.* **91** 170601
Nalbach P and Thorwart M 2009 arxiv:0911.5590
[24] Mohseni M *et al* 2008 *J. Chem. Phys.* **129** 174106
[25] Plenio M B and Huelga S F 2008 *New J. Phys.* **10** 113019
[26] Caruso F, Huelga S F and Plenio M B 2010 arXiv:1003.5877
[27] Cho M *et al* 2005 *J. Phys. Chem.* B **109** 10542
[28] Gaab K M and Bardeen C J 2004 *J. Chem. Phys.* **121** 7813
[29] Perdomo A *et al* 2010 arXiv:1001.2602 [quant-ph]
[30] Collini E *et al* 2010 *Nature* **463** 644
[31] Brandes T and Renzoni F 2000 *Phys. Rev. Lett.* **85** 4148
[32] Emary C 2007 *Phys. Rev.* B **76** 245319
[33] Arimondo E and Orriols G 1976 *Lett. Nuovo Cimento* **17** 333
[34] Lloyd S 2009 *Nat. Phys.* **5** 164
[35] Lee H, Cheng Y-C and Fleming G R 2007 *Science* **316** 1462
[36] Collini E and Scholes G D 2009 *Science* **323** 369
[37] Fassioli F *et al* 2009 arXiv:0907.5183
[38] Prior J *et al* 2010 arXiv:1003.5503
[39] Rebentrost P *et al* 2010 *J. Chem. Phys.* **131** 184102
[40] Thorwart M *et al* 2009 *Chem. Phys. Lett.* **478** 234
[41] Dijkstra A G and Tanimura Y 2010 arXiv:1004.1450
[42] Cramer M and Plenio M B 2010 arXiv:1002.3780
Flammia S T *et al* 2010 arXiv:1002.3839